Nanotechnology **20** (2009) 434005 (10pp) doi:10.1088/0957-4484/20/43/434005

# The stabilization and targeting of surfactant-synthesized gold nanorods

**Betty C Rostro-Kohanloo[1], Lissett R Bickford[2], Courtney M Payne[4], Emily S Day[2], Lindsey J E Anderson[1], Meng Zhong[3], Seunghyun Lee[4], Kathryn M Mayer[1], Tomasz Zal[5], Liana Adam[3], Colin P N Dinney[3], Rebekah A Drezek[2], Jennifer L West[2] and Jason H Hafner[1,4]**

[1] Department of Physics and Astronomy, Rice University, 6100 Main Street, Houston, TX 77005, USA
[2] Department of Bioengineering, Rice University, 6100 Main Street, Houston, TX 77005, USA
[3] Department of Urology, MD Anderson Cancer Center, 1515 Holcombe Boulevard, Houston, TX 77030, USA
[4] Department of Chemistry, Rice University, 6100 Main Street, Houston, TX 77005, USA
[5] Department of Immunology, MD Anderson Cancer Center, 1515 Holcombe Boulevard, Houston, TX 77030, USA

Received 6 May 2009
Published 2 October 2009
Online at stacks.iop.org/Nano/20/434005

**Abstract**
The strong cetyltrimethylammonium bromide (CTAB) surfactant responsible for the synthesis and stability of gold nanorod solutions complicates their biomedical applications. The critical parameter to maintain nanorod stability is the ratio of CTAB to nanorod concentration. The ratio is approximately 740 000 as determined by chloroform extraction of the CTAB from a nanorod solution. A comparison of nanorod stabilization by thiol-terminal PEG and by anionic polymers reveals that PEGylation results in higher yields and less aggregation upon removal of CTAB. A heterobifunctional PEG yields nanorods with exposed carboxyl groups for covalent conjugation to antibodies with the zero-length carbodiimide linker EDC. This conjugation strategy leads to approximately two functional antibodies per nanorod according to fluorimetry and ELISA assays. The nanorods specifically targeted cells *in vitro* and were visible with both two-photon and confocal reflectance microscopies. This covalent strategy should be generally applicable to other biomedical applications of gold nanorods as well as other gold nanoparticles synthesized with CTAB.

## Abbreviations

| | |
|---|---|
| Ab | antibody |
| AF-Ab | Alexa Fluor labeled antibody |
| CCD | charge coupled device |
| CTAB | cetyltrimethylammonium bromide |
| EDC | 1-ethyl-[3-dimethylaminopropyl]carbodiimide |
| ELISA | enzyme linked immunosorbent assay |
| HRP | horse radish peroxidase |
| LSPR | localized surface plasmon resonance |
| MES | 2-(*N*-morpholino)ethanesulfonic acid (MES) |
| NHS | *N*-hydroxysuccinimide |
| PBS | phosphate buffered saline |
| PEG | poly(ethylene glycol) |
| PSS | poly(sodium 4-stryene-sulfonate) |
| WGA | wheat germ agglutinin |

## 1. Introduction

Localized surface plasmon resonances (LSPR) of gold nanoparticles result in strong optical absorption and scattering at visible and near-infrared wavelengths [1]. These optical properties are of considerable interest for biomedical applications, since the plasmon resonance can affect localized heating and light scattering, and since gold nanoparticles are relatively inert in biological systems. Tunable gold nanoparticles have been recently investigated for applications in photothermal therapy, drug delivery and diagnostic imaging [2–8]. Biomedical applications will ultimately rely on the ability to target the gold nanoparticles specifically to certain tissues or cell types with antibodies, aptamers and peptides [9]. A variety of gold nanoparticle shapes have been fabricated and investigated, including spheres [10],

 

shells [11], rods [12–18], cages [19, 20] and stars [21]. One nanoparticle synthesis that is particularly powerful and versatile is the growth of colloidal gold seeds in the presence of the surfactant cetyltrimethylammonium bromide (CTAB). This method produced gold nanorods at first in low yield [22], and then later in high yield [23, 24] with resonances in the near-infrared. Gold nanorods are of particular interest for biomedical applications due to their small size and potentially improved permeation into tissue, relative to larger tunable gold nanoparticles. However, gold nanorods and other shapes synthesized with CTAB are also stabilized by this strong surfactant, which is thought to form a bilayer on the nanoparticle surface [25]. If the CTAB is removed from solution, the nanorods immediately aggregate [17]. Several strategies have been developed to modify the surface chemistry of nanorods, including polyelectrolyte wrapping to bind the CTAB layer [26], displacement of the CTAB layer by a thiol-terminal polyethylene glycol (PEG) [17] and displacement by alkanethiols [27] and lipids [28]. Even with these options, manipulation and targeting of nanorods has proven difficult, although there has been some recent success with polyelectrolyte wrapping [9, 12, 29–37]. This report describes progress on three aspects of biological targeting of CTAB-synthesized gold nanorods. First, the sensitivity of nanorod stability to CTAB concentration has been carefully characterized. Second, a simple chemical strategy has been developed to create nanorod–antibody conjugates based on strong gold–thiol and amide bonds that specifically target cells. Third, optical imaging modalities to detect nanorods in cells have been compared.

## 2. Materials and methods

### *2.1. Nanorod synthesis*

Gold nanorods were prepared as described previously [23, 24], but the procedure was scaled up to increase the quantity. All solutions were prepared fresh for each synthesis, except for the hydrogen tetrachloroaurate(III) (Sigma, #520918), which was prepared as a 28 mM stock solution from a dry ampule and stored in the dark. An aliquot of the stock solution was diluted to 10 mM immediately before use. Gold seed particles were prepared by adding 250 $\mu$l of 10 mM hydrogen tetrachloroaurate(III) to 7.5 ml of 100 mM cetyltrimethylammonium bromide (CTAB) (Sigma, #H9151) in a plastic tube with brief, gentle mixing by inversion. Next, 600 $\mu$l of 10 mM sodium borohydride (Acros, #18930) was prepared from DI water chilled to 2–8 °C in a refrigerator and added to the seed solution *immediately* after preparation, followed by mixing by inversion for 1–2 min. The pale brown seed solution was stable and usable for several hours.

The nanorod growth solution was prepared by adding the following reagents to a plastic tube in the following order and then gently mixing each by inversion: 425 ml of 100 mM CTAB, 18 ml of 10 mM hydrogen tetrachloroaurate(III) and 2.7 ml of 10 mM silver nitrate (Acros, #19768). Next, 2.9 ml of 100 mM ascorbic acid (Fisher, #A61) was added and mixed by inversion, which changed the solution from brownish-yellow to colorless. To initiate nanorod growth, 1.8 ml of seed solution was added to the growth solution, mixed gently by inversion and left still for three hours. During this time, the color changed gradually to dark purple, with most of the color change occurring in the first hour.

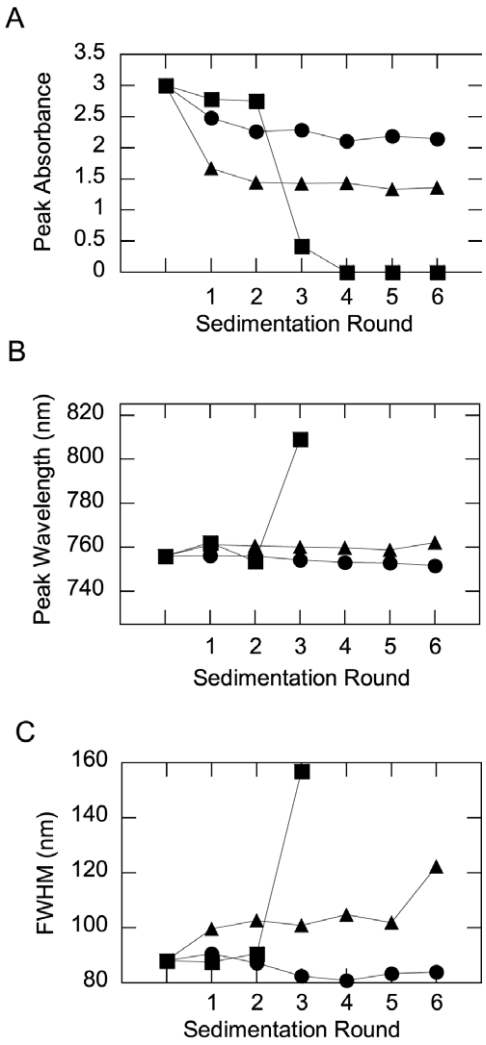


**Figure 1.** The evolution of the plasmon resonant peak of nanorod solutions after reduction of the CTAB concentration by sedimentation. The absorbance peak height (A), peak wavelength (B) and peak width (C) for CTAB-stabilized gold nanorods (■), anionic polymer-stabilized gold nanorods (▲) and PEGylated nanorods (●).

### *2.2. Nanorod stabilization*

Nanorod solutions were heated to 30 °C to melt CTAB crystals which form at room temperature, and therefore provide a known initial CTAB concentration of 100 mM. 5 ml aliquots were pelleted by centrifugation at 6000 rpm for 60 min. 4.5 ml of the clear supernatants were decanted and the pellets were resuspended with water. The nanorod solutions were pelleted again at 6000 rpm for 60 min and the clear supernatants were decanted. For anionic polymer stabilization, the nanorod pellets were resuspended with 4.5 ml of a solution containing 30 mg ml$^{-1}$ poly(sodium 4-styrene-sulfonate) (PSS, Aldrich, #243051) and 1 mM NaCl. For PEGylation, the nanorod pellets were resuspended with 4.5 ml

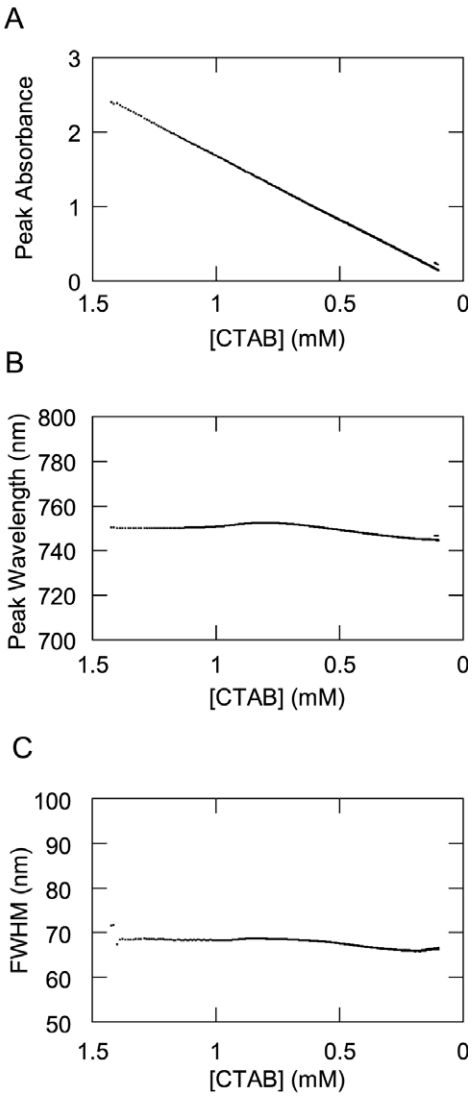


**Figure 2.** The evolution of the plasmon resonant peak height (A), wavelength (B) and width (C) of a nanorod solution during dilution with water.

of a solution containing 200 $\mu$M $K_2CO_3$ and 10 $\mu$M mPEG-SH (Nektar Therapeutics, #2M4E0H01). For both stabilization methods, the nanorod solution was incubated overnight at room temperature. Subsequent rounds of sedimentation, decantation and resuspension with water were then carried out as described above to lower the CTAB concentration.

### *2.3. CTAB dilution*

CTAB dilution was carried out by two methods. For the data in figure 1, the CTAB was diluted by subsequent rounds of sedimentation, decantation and resuspension with water as described in the preceding section, except that no stabilizing agent was applied. For the data in figure 2, a 600 $\mu$l aliquot of nanorods diluted to 1.4 mM CTAB was put in a custom 9 ml cuvette for spectral analysis. The plasmon resonant spectral extinction was monitored as water was added to the solution at 20 $\mu$l min$^{-1}$ with a pipette pump.

### *2.4. Chloroform extraction*

A separation funnel was filled with 100 ml of chloroform and 10 ml of nanorod solution which contained 30 mM CTAB. The mixture was vigorously shaken and allowed to separate overnight. The aqueous nanorod solution was extracted and 500 $\mu$l aliquots were placed in test tubes. To these tubes were added increasing quantities of chloroform for a second extraction: 0, 50, 100, 150, 200, 250 and 300 $\mu$l. After vigorous mixing, these were allowed to separate overnight. The aqueous nanorod solutions were then removed and analyzed.

### *2.5. Nanorod bioconjugation*

Nanorods were stabilized with the heterobifunctional linker $\alpha$-thio-$\omega$-carboxy poly(ethylene glycol) (Iris Biotech, #HOOC-PEG-SH) by the PEGylation method described above and resuspended in 100 mM 2-(*N*-morpholino)ethanesulfonic acid (MES) buffer (Sigma, #M-0164) at pH 6.1. The nanorods were concentrated by sedimentation to a volume of 100 $\mu$l with an absorbance value greater than 10 at the LSPR peak wavelength. 96 mg of 1-ethyl-[3-dimethylaminopropyl]carbodiimide (EDC, Sigma, #1769) and 29 mg of *N*-hydroxysuccinimide (NHS, Sigma, #1306762) were added to 10 ml of MES buffer, mixed and then 10 $\mu$l of this solution was immediately added to the 100 $\mu$l nanorod solution. This mixture was allowed to sit for 15 min, during which 0.5 ml of 2-mercaptoethanol was diluted into 14.5 ml MES buffer. After 15 min incubation, 10 $\mu$l of the diluted 2-mercaptoethanol was added to the nanorod solution. This mixture was allowed to sit for 10 min, after which 400 $\mu$l of the antibody solution at 2 mg ml$^{-1}$ in PBS pH 7.1 was added. This final 500 $\mu$l NR/Ab solution was incubated for 2 h at room temperature. Finally, the NR–Ab conjugates were separated from excess reactants and by-products by sedimentation at 10 000 rpm, decantation and resuspension of the pellet in PBS buffer.

### *2.6. Fluorimetry*

The procedure above was followed with an Alexa Fluor 488-labeled rabbit IgG (AF-Ab, Invitrogen, #A11059). Upon completion, the AF-Ab–NR conjugates were put through subsequent rounds of sedimentation, 90% decantation and resuspension in PBS. The supernatants and the final AF-Ab–NR conjugate solutions were analyzed in a Horiba Jobin-Yvon FluoroLog-3 fluorimeter with CW xenon excitation. The free AF-Ab in the supernatants served as a standard curve to determine the concentration of AF-Ab bound to the nanorods.

### *2.7. Nanoparticle ELISA*

Gold nanorods conjugated to mouse anti-human HER2 antibodies (NeoMarkers, #MS-301-PABX) were incubated with HRP-labeled anti-mouse IgG (Sigma, #A4416) for 1 h. Nonspecific reaction sites were blocked with a 3% solution of bovine serum albumin (BSA). Nanorods were rinsed twice by sedimentation and resuspension in 3% BSA to remove any unbound IgG. The HRP bound to the nanorod conjugates was

developed with 3, 3′, 5, 5′-tetramethylbenzidine dihydrochloride (Sigma, #T3405) and compared with an HRP anti-mouse IgG standard curve by determining the absorbance at 450 nm with a spectrophotometer.

### *2.8. Nanorod targeting*

Anti-HER2 nanorod conjugates were incubated with two cell types: the HER2-overexpressing epithelial breast cancer cell line SK-BR-3 and the normal mammary epithelial cell line MCF10A (American Type Culture Collection). The SK-BR-3 cells were grown in McCoy's 5A medium supplemented with 10% fetal bovine serum (FBS) and 1% penicillin–streptomycin and maintained at 37 °C in a 5% $CO_2$ atmosphere. The MCF10A cells were cultured in mammary epithelial basal medium (MEBM) supplemented with a BulletKit (Clonetics) and also maintained at 37 °C in 5% $CO_2$. Both cell lines were prepared for the experiment by putting $6 \times 10^5$ cells in chambered cover slips and allowing them 30 min to attach to the surface. The cells were rinsed once with PBS, then incubated with nanorod conjugates for 1 h in 5% $CO_2$ at 37 °C. The LSPR peak absorbance of the nanorod conjugate solutions was 1.5. After the incubation, cells were rinsed 3× with 1× PBS and then the appropriate cell medium was added prior to imaging. The cells were imaged by two-photon microscopy at 50× with 780 nm illumination and 400–700 nm detection.

KU7 cells were grown in MEM medium supplemented with 10% fetal bovine serum (FBS) and 1% penicillin–streptomycin and maintained at 37 °C in a 5% $CO_2$ atmosphere. The cell line was prepared for the experiment by putting $4 \times 10^5$ cells on cover slips and allowing them 24 h to attach to the surface. Prior to the treatment, the cell media was changed to OptiMEM (Roche Biochemicals) and nanorod-C225 conjugates were added for 4 h. After 4 h, the OptiMEM medium was changed to MEM medium supplemented with 10% serum and incubated in 5% $CO_2$ at 37 °C atmosphere for another 20 h. Twenty minutes prior to fixation, the cells were rinsed once with warm PBS, then incubated with 100 nM Alexa-488-wheat germ agglutinin (WGA) and left for 10 min in the cell incubator for WGA cellular internalization. After 10 min the cells were rinsed three times with warm PBS, fixed in 1:1 methanol:ethanol at 20 °C for 10 min, then washed three times with cold PBS and mounted on slides using slow-fade antifade. All reagents were purchased from Molecular Probes. Imaging was carried out with a Leica SP5RS AOBS confocal microscope using a 63×/1.4 objective. Nanorods were detected with 633 nm illumination in reflection mode. WGA-AF488 was excited at 488 nm and detected at 495–530 nm.

## 3. Results

### *3.1. Nanorod stability*

In order to determine the critical CTAB concentration required for nanorod stability, nanorod solutions were heated to melt the CTAB crystals and provide a well-defined initial concentration of 100 mM. Aliquots of nanorods were then pelleted by sedimentation, 90% of the clear supernatant was removed and the nanorod pellets were resuspended to their initial volume with water. In this way the CTAB concentration was reduced by a factor of 10 on each round of sedimentation. Note that the quantity of CTAB bound to the nanorod surfaces is a negligible fraction of this initial CTAB concentration[6]. The LSPR peak wavelength, width and height were recorded after each round of sedimentation and are plotted in figure 1. There was essentially no nanorod aggregation, i.e. no LSPR peak height reduction, broadening, or redshift, until the third round of sedimentation. Therefore, nanorod aggregation is expected to occur somewhere between 1 and 0.1 mM CTAB.

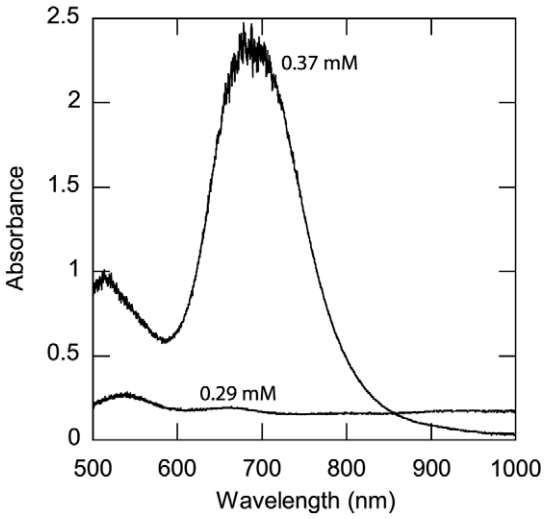


**Figure 3.** The plasmon resonant extinction spectra of nanorod solutions at two CTAB concentrations achieved by chloroform extraction. The nanorod concentration was 0.5 nM.

To further characterize the critical CTAB concentration, the LSPR spectrum of a nanorod solution was monitored during slow dilution with water (figure 2). As expected, the LSPR peak absorbance decreased as the nanorod concentration was reduced. However, the LSPR peak wavelength and width were not affected, indicating that there was no aggregation, although the CTAB concentration was reduced to below 50 $\mu$M. This apparent inconsistency with the results of figure 1 reveals that it is the ratio of CTAB concentration to nanorod concentration that determines stability, not the CTAB concentration alone, which is typical for surfactant-stabilized colloids. To further confirm this point, CTAB was removed from a nanorod solution without reducing the nanorod concentration by extraction with chloroform. As seen in figure 3, there was a critical CTAB concentration at which aggregation occurred. Based on our own measurement of the distribution ratio for CTAB between water and chloroform, the aggregation occurred between 370 and 290 $\mu$M CTAB. Given that the nanorod concentration was 0.5 nM, the critical CTAB/nanorod concentration ratio was approximately 740 000. Note that this number of CTAB molecules per

[6] Consider the typical conditions of a nanorod solution with $l = 50$ nm, $d = 15$ nm nanorods at an LSPR peak absorbance of 1, which corresponds to a nanorod concentration of 0.2 nM. The nanorod surface area would be 3063 nm$^2$. The CTAB bilayer packing area is 22 Å$^2$. Therefore, each nanorod would contain 14 000 CTAB molecules on its surface, taking up only 2.8 mM of the CTAB concentration.

**Table 1.** Zeta potential measurements to confirm surface chemistry modification.

| Nanoparticle | ZP (mV) |
|---|---|
| NR–CTAB | +83 |
| NR–S-PEG-COOH | −19 |
| NR–S-PEG-Ab | −6 |

nanorod is much larger than the amount of CTAB needed to simply coat the nanorods with a surfactant bilayer (see the footnote above), so the dynamic interactions between CTAB in solution and in the bilayer must be important for nanorod stability.

Nanorods were stabilized by displacement of the CTAB with a thiol-terminal polyethylene glycol (mPEG-SH), and by wrapping the CTAB bilayer with polystyrene sulfonate (PSS). The LSPR peak wavelength, width and height after successive rounds of sedimentation are displayed in figure 1 to probe the effectiveness of these stabilizers. While the unstabilized nanorods aggregated after the third round of sedimentation as described above, both PEGylation and polyelectrolyte stabilization were effective. However, PEGylation maintained a narrower LSPR peak, indicating a reduced degree of aggregation relative to polyelectrolyte stabilization.

### *3.2. Nanorod bioconjugation*

To form stable nanorod bioconjugates, a heterobifunctional polyethylene glycol with thiol and carboxyl end groups (HOOC-PEG-SH) was applied. Nanorod stabilization with HOOC-PEG-SH yielded identical results to mPEG-SH in figure 1. The carboxy-terminal nanorods were conjugated to antibodies using the zero-length crosslinker EDC stabilized by NHS [38]. Standard procedures for EDC protein crosslinking were followed [39], with the following modifications for the unique properties of the carboxy-terminal nanorods. First, since the functionalized nanorod surfaces contain no amines, there is no chance of nanorod aggregation due to amide bond formation between nanorods, which minimizes the criticality of the initial EDC exposure. Second, to avoid the need for buffer exchange or sedimentation, the change in pH from 6.1 for activation to 7.1 for conjugation was accomplished by diluting the nanorods into a larger volume of antibody solution. Finally, sedimentation was performed (rather than buffer exchange) to remove excess reactants and products from the nanorod solution.

As a means to confirm the altered nanorod surface chemistry at various stages, zeta potential measurements (Malvern Zetasizer Nano) were performed on gold nanorods in the original CTAB, after stabilization with HOOC-PEG-SH, and finally after Ab conjugation. The results, presented in table 1, are consistent with the cationic, anionic and zwitterionic surface charges, respectively, associated with these three states of nanorods.

To characterize the final product, nanorods were conjugated to AF-Ab for fluorimetric analysis. After the steps described above, the nanorod conjugates were put through successive rounds of sedimentation, 90% decantation and resuspension in buffer to dilute the unbound AF-Ab by factors of ten. Fluorimetry of unbound AF-Ab in the decants, shown in figure 4, serves as a standard curve and reaches the background fluorescence noise floor by the fourth round at an AF-Ab concentration of 0.1 nM. Fluorimetry of the nanorod conjugates solution indicated a nanorod-bound AF-Ab concentration of 1 nM, which yields approximately two antibodies per nanorod given a nanorod concentration of 0.5 nM based on the LSPR extinction peak [17].

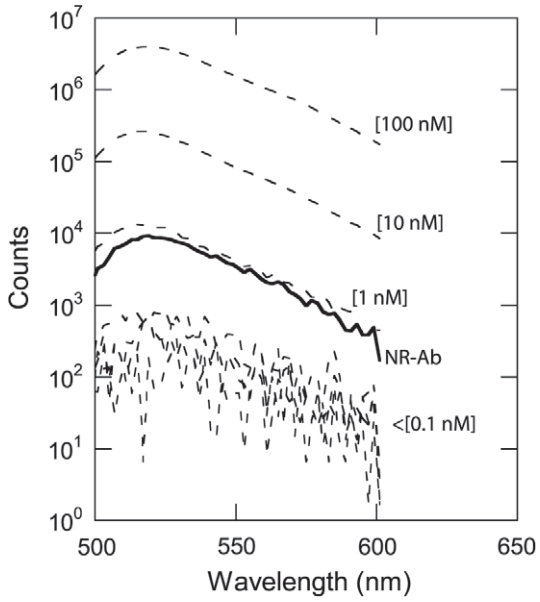


**Figure 4.** Fluorimetric analysis of gold nanorod conjugates. The dashed curves display the signal from free labeled antibodies in solution at the stated concentrations. The solid curve displays the signal from nanorod conjugates.

To further characterize the nanorod conjugates, a nanoparticle ELISA was performed [40]. This method is similar to a traditional ELISA except that the immunosorbent surface is that of the nanoparticles in solution. The nanoparticle ELISA yielded 2.28 ± 0.05 antibodies per nanorod, in reasonable agreement with the fluorimetry results. A simultaneous ELISA on nanorods prepared with mPEG-SH, and therefore no capture antibodies, yielded 0.68 ± 0.2 antibodies per nanorod. This signal may be an artifact due to chemisorption of the label antibody to the available gold surface on the nanorods.

### *3.3. Nanorod targeting and imaging*

Nanorod conjugate targeting was tested with two *in vitro* systems. First, nanorods were conjugated to anti-HER2 and also to rabbit IgG as a control. Each conjugate was incubated with both the HER2-overexpressing epithelial breast cancer cell line SK-BR-3 and the normal mammary epithelial cell line MCF10A for 30 min simultaneously and under identical conditions. The cells were washed and immediately imaged live by two-photon luminescence, which highlights the presence of gold particles [18], as well as phase contrast to show the cell locations. Figure 5 demonstrates that only the specific antibody/cell combination produced a significant level

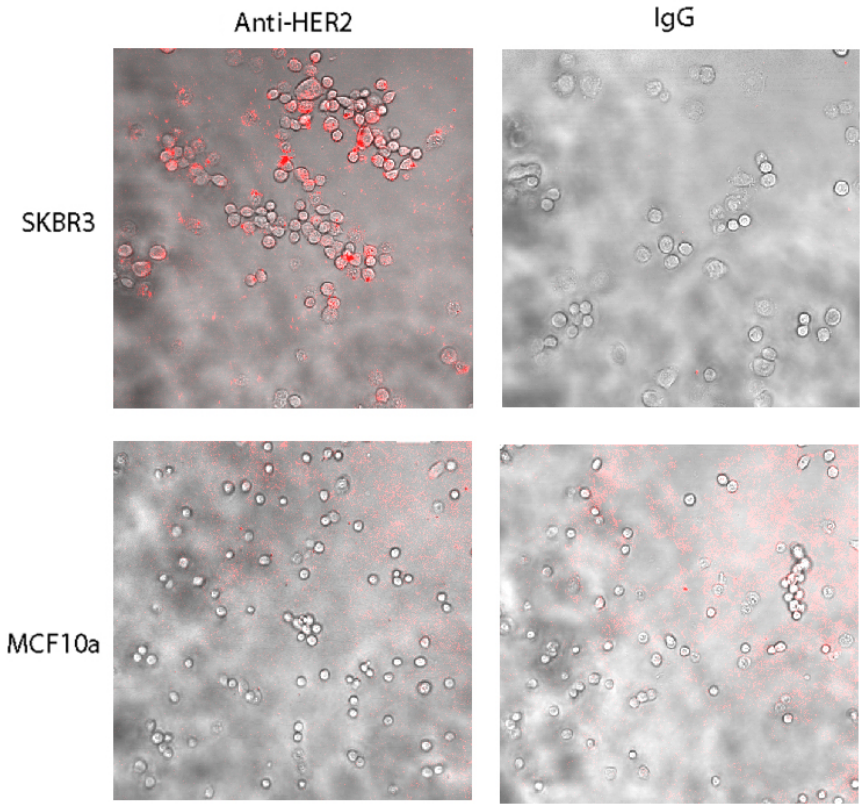


**Figure 5.** Nanorod conjugate targeting. Phase contrast shows the cell locations in grayscale, and two-photon luminescence is displayed in red. Binding was only observed for the anti-HER2 conjugates and SKBR3 cells.

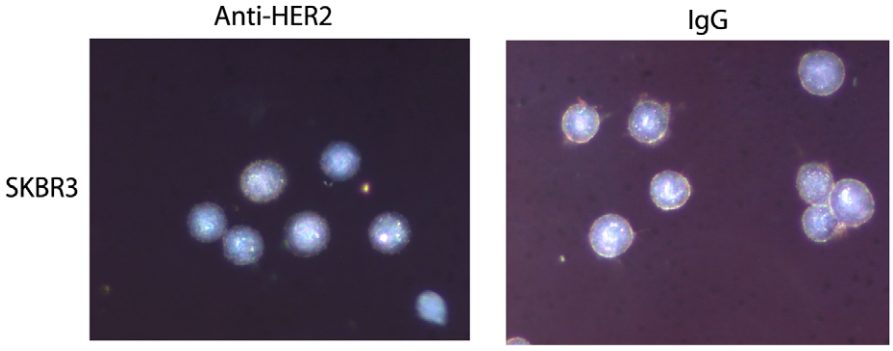


**Figure 6.** Dark-field microscopy images of the same samples as in figure 5.

of nanorod binding to the cells. Figure 6 displays dark-field images of targeted and control cells from the same sample. The nanorods were not visible. To gauge their visibility in dark-field microscopy, isolated nanorods were deposited on glass substrates near alignment marks and easily visible spherical gold nanoparticles so that optical microscopy and AFM could be performed on the same area (see figure 7). The nanorod was not detectable on either a high-sensitivity monochromator or color CCD cameras.

The conjugation method was also tested with C225 and human IgG as a control. In this case, the nanorod conjugates were incubated with the KU7 bladder cancer cell line. The nanorods were imaged by confocal reflectance and the cells were visualized with a fluorescent WGA label. The C225 conjugates were more strongly associated with KU7 cells than the control IgG conjugates, as seen in figure 8.

## 4. Discussion

It is well known that the CTAB surfactant responsible for gold nanorod synthesis is also required to maintain colloidal stability. However, the CTAB concentration at which colloidal stability is lost has not been well characterized. This is due to several factors. First, to reduce the CTAB concentration in a nanorod solution, it is often removed by sedimentation of the nanorods into a pellet, decantation of the CTAB solution and resuspension of the nanorod pellet in water. If this procedure is not performed analytically, the CTAB concentration is

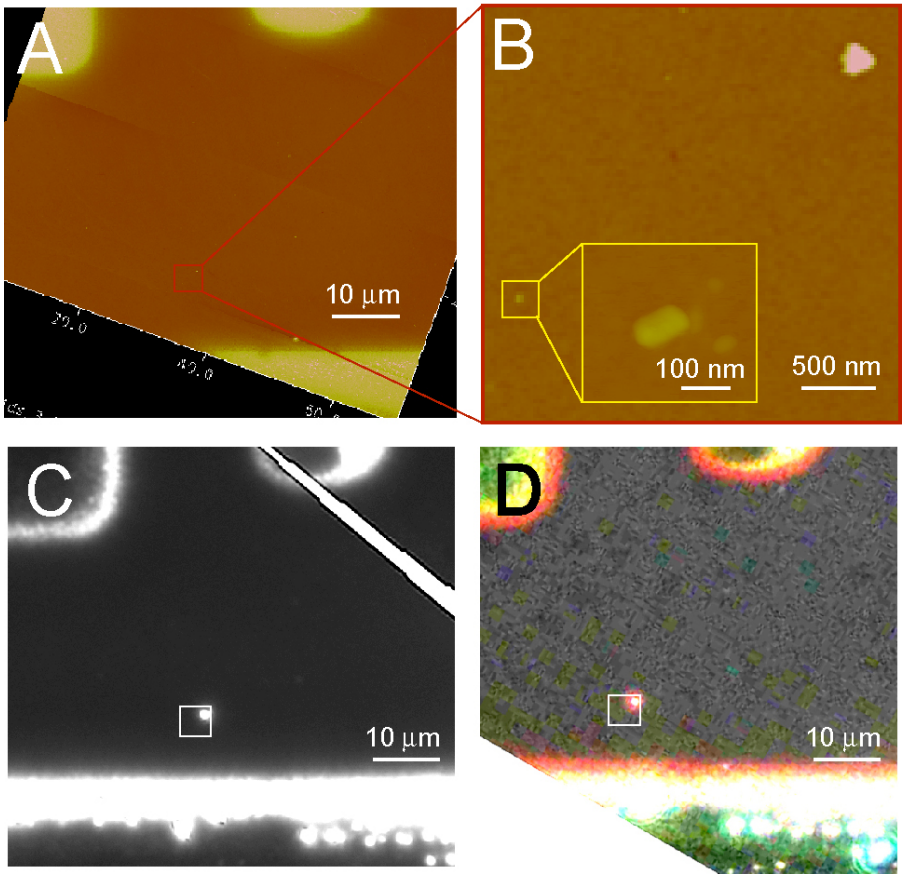


**Figure 7.** Dark-field microscopy images of a single gold nanorod on glass. The first AFM image (A) shows a region near alignment marks that are also visible in the optical images ((C) and (D)). A zoomed AFM image (B) reveals a large nanosphere in the upper right (triangular shape is a tip artifact) and a nanorod in the lower left. The nanorod is clearly revealed in the inset. Its size is exaggerated by the tip. The true size is approximately 50 nm length and 15 nm width. Dark-field images captured with a high-sensitivity CCD (C) and color CCD (D) clearly show the nanosphere, but show no sign of the nanorod in the expected region, even with significant contrast enhancement. The inset boxes in (A), (C) and (D) are all shown at the same size and position.

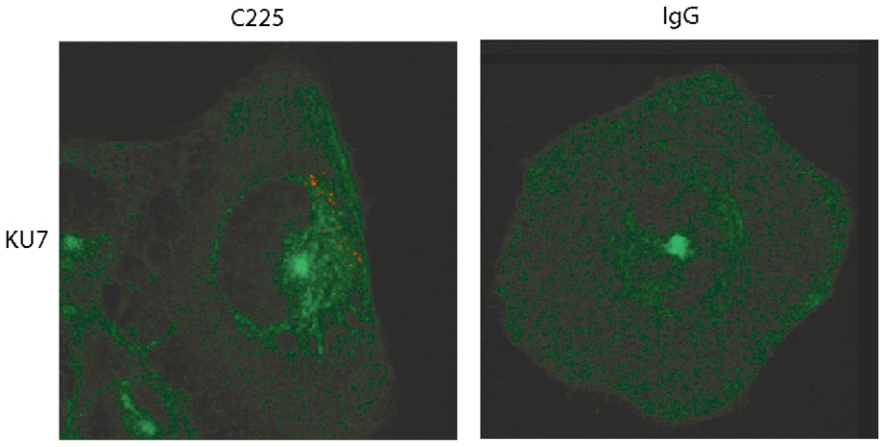


**Figure 8.** *In vitro* nanorod imaging by confocal reflectance. WGA-AF488 fluorescence shows the cell location in green and confocal reflectance at 633 nm is shown in red. Nanorod binding is only observed for the specific C225 conjugates and KU7 cells.

reduced by an unknown amount. Second, nanorod synthesis is carried out at 100 mM CTAB, which is above the saturation concentration at room temperature. Upon storage, some of the CTAB crystallizes, leaving an unknown concentration in the nanorod solution drawn from the solution phase. Finally, attempts at spectroscopic or other analyses of the CTAB concentration are hindered by micellization and association with gold and silver ions in solution.

That the nanorods were found to be entirely stable to a CTAB concentration below 1 mM may confound the development of methods to stabilize nanorods, since the CTAB may stabilize the nanorods when it is thought to have been

removed. Nanorod stabilization outside of the CTAB solution is further complicated by several factors. First, the aggregation occurs quite suddenly when the CTAB concentration falls below the critical value, as seen in figure 3. Second, the fact that it is the ratio of CTAB to nanorod concentration that determines stability, rather than the CTAB concentration alone, means that the critical CTAB concentration for a given sample will depend on the nanorod concentration. Third, since CTAB forms a bilayer on the nanorod surface, it is likely that the available nanorod surface area is critical for stability rather than the nanorod concentration. Therefore, the critical CTAB concentration for a given sample also depends on nanorod size. This significant variability of the critical CTAB concentration between samples may in part account for reproducibility issues in stabilizing gold nanorods and forming bioconjugates.

We previously described a strategy to stabilize gold nanorods with a thiol-terminal polyethylene glycol (mPEG-SH) which displaces the CTAB bilayer so that CTAB can be reduced to an arbitrarily low concentration and the nanorods remain in solution [17]. Nanorods can also be stabilized by wrapping them with anionic polymers which are attracted to the cationic CTAB bilayer, as well as by forming multiple polyelectrolyte layers [26]. Figure 1 displays a comparison of the effectiveness of these methods for stabilizing nanorods. Interestingly, after the first and second rounds of sedimentation, the sample with no stabilizing treatment maintained the best spectrum, although aggregation occurred rapidly thereafter. The data demonstrate that, upon removal of CTAB, PEGylation via the thiol–gold bond results in higher yields and a narrower LSPR linewidth than electrostatic stabilization. This spectroscopic result is in agreement with previously reported microscopic characterizations of nanorod substrates. PEGylated nanorod solutions yield highly monodisperse nanorods when deposited on glass substrates [17], while electrostatic wrapping leads to aggregated nanorods [26].

Most gold nanorod targeting experiments to date have been carried out by stabilizing the CTAB-capped gold nanorods with polyelectrolytes, then non-covalently binding antibodies or other targeting agents to the nanoparticles by simply mixing them together [12, 29, 31–33, 35, 36]. This is similar to the original strategies developed to bind antibodies to citrate-capped gold nanoparticles for immunoelectron microscopy [41]. The binding is likely due to weak electrostatic and hydrophobic interactions between the nanoparticles and antibodies. To create more stable nanorod bioconjugates, the strategy described here relies on an amide bond between the linker and antibody, and a strong gold–thiol bond [42] between the linker and nanorod. In some cases polyelectrolytes with exposed carboxyl groups for amide bond formation with antibodies have been employed [30, 37]. In one case an alkanethiol was used in a similar manner to the bifunctional PEG described here [43]. While alkanethiols are more readily available, their low solubility in aqueous solutions required hours of sonication at elevated temperature to achieve sufficient concentration to displace the CTAB bilayer. Although more complicated, conjugates based on gold–thiol and covalent bonds will likely be more stable for *in vivo* applications. Furthermore, we have found the methods described here to be quite reproducible despite the strength of the original gold–CTAB interaction [12]. Tests of the nanorod zeta potential follow the intended surface chemistry, with a negative potential for carboxy-terminated nanorods and a near-neutral potential for the zwitterionic protein conjugates. The fluorimetric assay yields approximately two antibodies per nanorod and the ELISA assay demonstrates that a large fraction of these antibodies are active. Finally, figures 5 and 8 demonstrate successful targeting in two cell types with different antibodies.

We have also investigated the effectiveness of different imaging modalities to visualize nanorods in and around cells. As described previously [18], the images based on two-photon luminescence in figure 5 clearly reveal nanorods in the specific sample. Dark-field microscopy is a much simpler modality that can yield striking images of plasmon resonant nanoparticles [44]. However, the optical scattering which provides dark-field contrast is a strong function of nanoparticle size. Furthermore, the size range at which nanoparticles become visible by dark-field is tens of nanometers, similar to the range of nanoparticles that have been pursued for biomedical applications. Issues of visibility are also sensitive to the illumination and imaging numerical apertures, spectral range, nanoparticle aggregation and background scattering from cells. Therefore, one must be cautious when interpreting nanoparticle targeting results by dark-field microscopy. For example, the dark-field images from figure 6 reveal no evidence of scattering by the nanorods, even though the two-photon images from figure 5 confirm the presence of nanorods. In this case the single 50 nm × 15 nm nanorods do not scatter sufficiently to be visible against the scattering from cells. To further confirm this point, dark-field images of a single nanorod on a glass substrate are displayed in figure 7. Although the location of a single gold nanorod relative to alignment marks is confirmed by atomic force microscopy, one finds that the nanorod is not visible in the dark-field images taken with either a color CCD camera or a back-illuminated electron multiplying CCD camera. If single nanorods are not visible on a flat glass substrate, it is not surprising that they are not visible in the higher background images of cells in figure 6. There are many methods to increase the nanorod imaging signal and contrast without resorting to two-photon luminescence, such as spectrally filtering the scattered light, exciting with monochromatic illumination at the plasmon resonant wavelength and using a higher numerical aperture condensers and objectives. Figure 8 reveals that confocal reflectance microscopy, with monochromatic illumination at the LSPR wavelength and reduced background signal, is sufficient to detect nanorods in cells.

## 5. Conclusions

To maintain colloidal stability, it is the ratio of CTAB to nanorod concentration that must be maintained. Here, the critical CTAB:nanorod ratio was found to be approximately 740 000:1. The CTAB layer can be displaced by thiol-terminal PEG, or wrapped by polyelectrolytes. However,

gold–thiol PEGylation results in higher yields and more monodisperse nanorod samples when the CTAB is removed. A bifunctional PEG with thiol and carboxyl end groups results in carboxy-terminal PEGylated nanorods which can be conjugated to antibodies via a carbodiimide linking agent. Fluorimetry and ELISA assays reveal approximately two antibodies per nanorod. The nanorod conjugates demonstrated specific targeting in two different antibody/cell systems. Two-photon luminescence and confocal reflectance microscopies successfully imaged the nanorods in cells.

## Acknowledgments

JHH acknowledges support from the National Science Foundation's Nanoscale Science and Engineering Initiative under award no. EEC-0647452, the US Army Research Office under grant no. W911NF-04-1-0203 and the Welch Foundation under grant C-1556. JHH and LA acknowledge support from the Department of Defense grant W81XWH-06-2-0067 to UTHSC. LJEA acknowledges support from the NSF-funded Integrative Graduate Research and Educational Training program DGE-0750842. RAD acknowledges support from the Department of Defense grant W81XWH-07-1-0428, and the Welch Foundation under grant C-1598.

## References

[1] Link S and El-Sayed M A 1999 Spectral properties and relaxation dynamics of surface plasmon electronic oscillations in gold and silver nanodots and nanorods *J. Phys. Chem.* B **103** 8410–26

[2] Liao H, Nehl C L and Hafner J H 2006 Biomedical applications of plasmon resonant metal nanoparticles *Nanomedicine* **1** 201–8

[3] Jain P K, Huang X H, El-Sayed I H and El-Sayed M A 2008 Noble metals on the nanoscale: optical and photothermal properties and some applications in imaging, sensing, biology, and medicine *Acc. Chem. Res.* **41** 1578–86

[4] Murphy C J, Gole A M, Stone J W, Sisco P N, Alkilany A M, Goldsmith E C and Baxter S C 2008 Gold nanoparticles in biology: beyond toxicity to cellular imaging *Acc. Chem. Res.* **41** 1721–30

[5] Lal S, Clare S E and Halas N J 2008 Nanoshell-enabled photothermal cancer therapy: impending clinical impact *Acc. Chem. Res.* **41** 1842–51

[6] Bikram M and West J L 2008 Thermo-responsive systems for controlled drug delivery *Expert Opin. Drug Deliv.* **5** 1077–91

[7] Tong L, Wei Q S, Wei A and Cheng J X 2009 Gold nanorods as contrast agents for biological imaging: optical properties, surface conjugation and photothermal effects *Photochem. Photobiol.* **85** 21–32

[8] Hleb E Y, Hu Y, Drezek R A, Hafner J H and Lapotko D O 2008 Photothermal bubbles as optical scattering probes for imaging living cells *Nanomedicine* **3** 797–812

[9] Pirollo K F and Chang E H 2008 Does a targeting ligand influence nanoparticle tumor localization or uptake? *Trends Biotechnol.* **26** 552–8

[10] Sokolov K, Follen M, Aaron J, Pavlova I, Malpica A, Lotan R and Richards-Kortum R 2003 Real-time vital optical imaging of precancer using anti-epidermal growth factor receptor antibodies conjugated to gold nanoparticles *Cancer Res.* **63** 1999–2004

[11] Loo C, Lowery A, Halas N, West J and Drezek R 2005 Immunotargeted nanoshells for integrated cancer imaging and therapy *Nano Lett.* **5** 709–11

[12] Javier D J, Nitin N, Roblyer D M and Richards-Kortum R 2008 Metal-based nanorods as molecule-specific contrast agents for reflectance imaging in 3D tissues *J. Nanophoton.* **2** 023506

[13] Yu C X, Nakshatri H and Irudayaraj J 2007 Identity profiling of cell surface markers by multiplex gold nanorod probes *Nano Lett.* **7** 2300–6

[14] Eghtedari M, Oraevsky A, Copland J A, Kotov N A, Conjusteau A and Motamedi M 2007 High sensitivity of *in vivo* detection of gold nanorods using a laser optoacoustic imaging system *Nano Lett.* **7** 1914–8

[15] Huff T B, Hansen M N, Zhao Y, Cheng J X and Wei A 2007 Controlling the cellular uptake of gold nanorods *Langmuir* **23** 1596–9

[16] Chen C C, Lin Y P, Wang C W, Tzeng H C, Wu C H, Chen Y C, Chen C P, Chen L C and Wu Y C 2006 DNA-gold nanorod conjugates for remote control of localized gene expression by near infrared irradiation *J. Am. Chem. Soc.* **128** 3709–15

[17] Liao H and Hafner J 2005 Gold nanorod bioconjugates *Chem. Mater.* **17** 4636–41

[18] Wang H, Huff T B, Zweifel D A, He W, Low P S, Wei A and Cheng J-X 2005 *In vitro* and *in vivo* two-photon luminescence imaging of single gold nanorods *Proc. Natl. Acad. Sci. USA* **102** 15752–6

[19] Cang H, Sun T, Li Z Y, Chen J Y, Wiley B J, Xia Y N and Li X D 2005 Gold nanocages as contrast agents for spectroscopic optical coherence tomography *Opt. Lett.* **30** 3048–50

[20] Skrabalak S E, Chen J, Au L, Lu X, Li X and Xia Y 2007 Gold nanocages for biomedical applications *Adv. Mater.* **19** 3177–84

[21] Nehl C L, Liao H W and Hafner J H 2006 Optical properties of star-shaped gold nanoparticles *Nano Lett.* **6** 683–8

[22] Jana N R, Gearheart L and Murphy C J 2001 Wet chemical synthesis of high aspect ratio cylindrical gold nanorods *J. Phys. Chem.* B **105** 4065–7

[23] Sau T K and Murphy C J 2004 Seeded high yield synthesis of short Au nanorods in aqueous solution *Langmuir* **20** 6414–20

[24] Nikoobakht B and El-Sayed M A 2003 Preparation and growth mechanism of gold nanorods (NRs) using seed-mediated growth method *Chem. Mater.* **15** 1957–62

[25] Nikoobakht B and El-Sayed M A 2001 Evidence for bilayer assembly of cationic surfactants on the surface of gold nanorods *Langmuir* **17** 6368–74

[26] Gole A and Murphy C J 2005 Polyelectrolyte-coated gold nanorods: synthesis, characterization and immobilization *Chem. Mater.* **17** 1325–30

[27] Sun Z H, Ni W H, Yang Z, Kou X S, Li L and Wang J F 2008 pH-controlled reversible assembly and disassembly of gold nanorods *Small* **4** 1287–92

[28] Niidome Y, Honda K, Higashimoto K, Kawazumi H, Yamada S, Nakashima N, Sasaki Y, Ishida Y and Kikuchi J 2007 Surface modification of gold nanorods with synthetic cationic lipids *Chem. Commun.* 3777–9

[29] Tong L, Zhao Y, Huff T B, Hansen M N, Wei A and Cheng J X 2007 Gold nanorods mediate tumor cell death by compromising membrane integrity *Adv. Mater.* **19** 3136

[30] Popovtzer R, Agrawal A, Kotov N A, Popovtzer A, Balter J, Carey T E and Kopelman R 2008 Targeted gold nanoparticles enable molecular CT imaging of cancer *Nano Lett.* **8** 4593–6

[31] Huang X H, El-Sayed I H, Qian W and El-Sayed M A 2007 Cancer cells assemble and align gold nanorods conjugated to antibodies to produce highly enhanced, sharp, and polarized surface Raman spectra: a potential cancer diagnostic marker *Nano Lett.* **7** 1591–7

[32] Huang X H, El-Sayed I H, Qian W and El-Sayed M A 2006 Cancer cell imaging and photothermal therapy in the near-infrared region by using gold nanorods *J. Am. Chem. Soc.* **128** 2115–20
[33] Hu R, Yong K T, Roy I, Ding H, He S and Prasad P N 2009 Metallic nanostructures as localized plasmon resonance enhanced scattering probes for multiplex dark-field targeted imaging of cancer cells *J. Phys. Chem.* C **113** 2676–84
[34] Hauck T S, Ghazani A A and Chan W C W 2008 Assessing the effect of surface chemistry on gold nanorod uptake, toxicity, and gene expression in mammalian cells *Small* **4** 153–9
[35] Durr N J, Larson T, Smith D K, Korgel B A, Sokolov K and Ben-Yakar A 2007 Two-photon luminescence imaging of cancer cells using molecularly targeted gold nanorods *Nano Lett.* **7** 941–5
[36] Ding H, Yong K T, Roy I, Pudavar H E, Law W C, Bergey E J and Prasad P N 2007 Gold nanorods coated with multilayer polyelectrolyte as contrast agents for multimodal imaging *J. Phys. Chem.* C **111** 12552–7
[37] Agarwal A, Huang S W, O'Donnell M, Day K C, Day M, Kotov N and Ashkenazi S 2007 Targeted gold nanorod contrast agent for prostate cancer detection by photoacoustic imaging *J. Appl. Phys.* **102** 064701
[38] Grabarek Z and Gergely J 1990 Zero-length crosslinking procedure with the use of active esters *Anal. Biochem.* **185** 131–5
[39] Hermanson G T 1996 *Bioconjugate Techniques* 1st edn (New York: Academic) p 785
[40] Lowery A R, Gobin A M, Day E S, Halas N J and West J L 2006 Immunonanoshells for targeted photothermal ablation of tumor cells *Int. J. Nanomed.* **1** 149–54
[41] Geoghegan W D and Ackerman G A 1977 Adsorption of horseradish-peroxidase, ovomucoid and antiimmunoglobulin to colloidal gold for indirect detection of concanavalin-a, wheat-germ agglutinin and goat antihuman immunoglobulin-g on cell-surfaces at electron-microscopic level—new method, theory and application *J. Histochem. Cytochem.* **25** 1187–200
[42] Nuzzo R G, Zegarski B R and Dubois L H 1987 Fundamental-studies of the chemisorption of organosulfur compounds on Au(111)—implications for molecular self-assembly on gold surfaces *J. Am. Chem. Soc.* **109** 733–40
[43] Eghtedari M, Liopo A V, Copland J A, Oraevslty A A and Motamedi M 2009 Engineering of hetero-functional gold nanorods for the *in vivo* molecular targeting of breast cancer cells *Nano Lett.* **9** 287–91
[44] Mock J J, Barbic M, Smith D R, Schultz D A and Schultz S 2002 Shape effects in plasmon resonance of individual colloidal silver nanoparticles *J. Chem. Phys.* **116** 6755–9